CHAPITRE 2

SUPERELASTICITY-RELATED PHENOMENA OF SHAPE MEMORY ALLOY PASSIVE DAMPERS[1]

2.1 Introduction

The particular SMA properties, notably the completely reversible phase transformation and the energy dissipation provided by the phase transformation, make them suitable for damping applications. Furthermore, the excellent corrosion resistance and the good fatigue properties of these alloys have led to them being used as passive dampers. Some applications have been proposed to retrofit historic buildings [67], to control displacement of bridges [65] and buildings [42;64;66], or as tendons in concrete structures [70]. In this study, some aspects of SMA will be investigated and simulated: the effect related to the heat produced and absorbed by the martensitic phase transformation and the influence of superelasticity-related properties (variation of stiffness and energy dissipated) under harmonic oscillations.

2.2 Self-heating effects

It is well known that SMA behavior is dependent on the strain rate [47;53;55]. A cause of that dependency is the heat produced (or absorbed) by the phase transformation. At a certain strain rate, there may not be sufficient time for the heat to be dissipated (or absorbed) and the temperature of the sample increases (or decreases): it is the so-called self-heating effect (SHE). Due to their thermomechanical nature, the mechanical

---

[1] Cet article de conférence a été présenté à l'« *International Conference on Shape Memory and Superelastic Technologies* » (SMST) à Asilomar (Californie) en mai 2006. Les auteurs sont Pierre Lafortune (ÉTS), Patrick Terriault (ÉTS), Vladimir Brailovski (ÉTS) et Vicenç Torra (*Universitat Politècnica de Catalunya*). Il est présentement à l'étape de révision par les pairs pour publication.

behavior of SMA will be affected by this SHE. These changes have to be considered, especially in the case of repeated cycles encountered in seismic applications [39;71].

For relatively low strain rates, different authors observed an increase of the direct transformation stress plateau and a lowering of the reverse transformation stress plateau, leading to a larger hysteresis width [49;50]. However other studies showed that for higher strain rates, the temperature increase of the sample is more significant, leading to a translation of the hysteretic loop toward higher stresses and to a reduction of the hysteresis width [44;46].

The aim of this section is to program the self-heating effect of SMA in a finite element model, and to validate this model with experimental tests.

2.2.1 Experimental study

2.2.1.1 Samples

Firstly, two types of small diameter NiTi wires (Ti 50.7at.%Ni) have been tested. The first group of wires has a diameter of 0.5 mm and has been heat treated (annealed at 400 °C for 30 minutes, water quenched and aged for 10 days at room temperature). The second group of wires has a diameter of 0.1 mm and is used as-supplied (Special Metals, USA). Both types of wires are used in their superelastic state. Prior to testing, each wire was pre-cycled for 50 cycles at 0.001 Hz up to 6% and 8 % strain respectively for the 0.5 mm and the 0.1 mm wires. The Clausius-Clapeyron slopes given in table 1 have been determined by performing several tensile tests at different temperatures above Af (austenite finish temperature).

Secondly, NiTi wires with a larger diameter of 2.46 mm have been tested. This type of wire is more realistic for the applications in civil engineering (working force per wire

close to 2 kN). Furthermore, the temperature measurement is easier with such a diameter. Partial results concerning these wires are presented in section 2.2.4.

2.2.2 Results for the small diameter wires

Several quasi-static and dynamic tensile tests are carried out on the wires with an Enduratec ELF 3200 tensile testing machine equipped with a 450 N load cell. The effective length of the wire is 60 mm. Strain rate of 0.001, 0.005 and 1 Hz are used for the 0.5 mm wires, while 0.005, 1 and 7 Hz are used for the 0.1 mm wires (figure 24). A test consists of only one complete cycle via a ramp-shaped loading-unloading sequence.

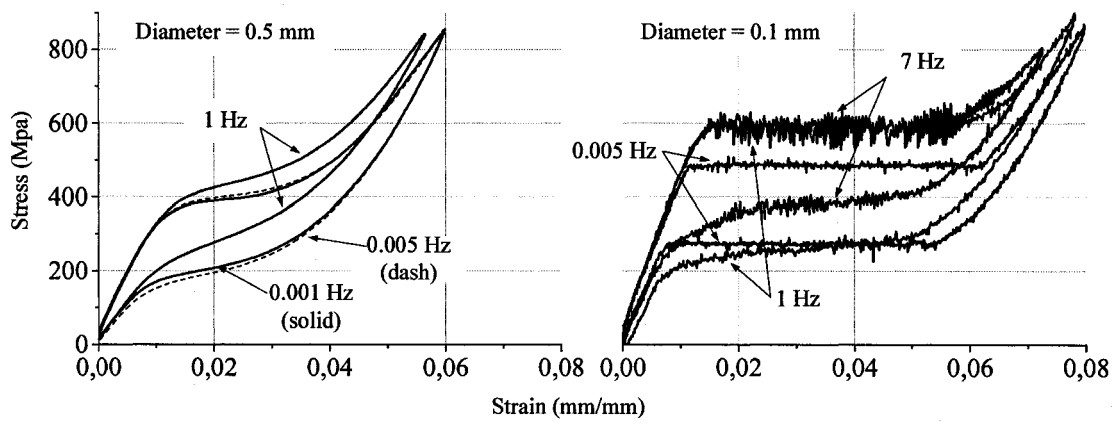

Figure 24 Stress-strain diagrams of the tested wires at different strain rates. Left: 0.5 mm diameter (0.001, 0.005 and 1 Hz). Right: 0.1 mm diameter (0.005, 1 and 7 Hz).

2.2.3 Simulations

2.2.3.1 Theory

In this section, the evolution of the temperature in a dynamically loaded wire is calculated. To do so, the concept of heat balance is used. If we assume, as a preliminary approach, that the temperature T of the wire is uniform at any time t, we have:

$$\dot{E}_g - \dot{E}_{out} = \dot{E}_{st} \tag{2-1}$$

where $\dot{E}_g$ is the energy rate generated in the volume, $\dot{E}_{out}$ is the energy rate dissipated to the surrounding and $\dot{E}_{st}$ is the energy rate stored in the volume.

The term of heat generation in equation (2-1) reflects the contribution of two phenomena, both assumed to be proportional to the fraction of martensite (ξ). The first contribution is due to recoverable latent heat (LH) associated with the phase transformation:

$$\dot{E}_{g(LH)} = \pm \frac{m \cdot \ell \cdot \Delta\xi}{\Delta t} \tag{2-2}$$

where m is the mass of the wire, ℓ is the enthalpy of transformation and $\Delta\xi$ is the increment or decrement of the martensite content that appeared or disappeared during the time increment Δt. The $\pm$ sign is due to the fact that the direct transformation is exothermic, while the reverse transformation is endothermic.

The second contribution is related to the irrecoverable internal friction (IF) produced by the motion of martensitic interfaces during the transformation [13;15]. This energy corresponds to the area inside the stress-strain hysteresis loop:

$$H = \oint \sigma \cdot d\varepsilon \tag{2-3}$$

For a volume V, the expression for the IF contribution is then:

$$\dot{E}_{g(IF)} = \frac{1}{2} \cdot \frac{V \cdot H \cdot \Delta\xi}{\Delta t} \tag{2-4}$$

The term H is assumed to be strain-rate independent and is then kept constant. It is also considered that half of H is dissipated during loading and the other half during unloading, which explains the factor ½.

The energy can leave the sample through the exchange area A_e proportionally to the difference between the wire temperature (T_i) and room temperature (T_∞):

$$\dot{E}_{out} = h \cdot A_e \cdot (T_i - T_\infty) \tag{2-5}$$

The coefficient h is the sum of the free convection exchange coefficient h_{conv} and the radiation exchange coefficient h_{rad}. h_{conv} is evaluated with correlations proposed in the literature [72], and has a value of 10 $W/(m^2 \cdot K)$. Since the difference $(T_i - T_\infty)$ is small, h_{rad} is approximated by [73]:

$$h_{rad} = 4 \cdot \sigma \cdot T^3 \tag{2-6}$$

where $\sigma = 5.67 \cdot 10^{-8}\ \mathrm{W/(m^2 \cdot K^4)}$ is the Stefan-Boltzmann constant. For a mean temperature of T = 303 K, h_{rad} gives 6.3 $\mathrm{W/(m^2 \cdot K)}$. The total value of h is then 16.3 $\mathrm{W/(m^2 \cdot K)}$.

Finally, the right hand term of equation (1) is expressed by:

$$\dot{E}_{st} = m \cdot c \cdot \frac{dT}{dt} \tag{2-7}$$

where c is the specific heat of NiTi. The differential relation dT/dt is evaluated using the explicit finite difference:

$$\frac{dT}{dt} \approx \frac{T_{i+1} - T_i}{\Delta t} \tag{2-8}$$

where the subscripts define the time at which the temperatures are evaluated. Solving equations (2-1) to (2-8) for T_{i+1} we obtain the temperature at time i+1:

$$T_{i+1} = T_i + \frac{\Delta \xi}{m \cdot c} \cdot (\pm m \cdot \ell + V \cdot H) - \frac{\Delta t \cdot h \cdot A_e}{m \cdot c} \cdot (T_i - T_\infty) \tag{2-9}$$

2.2.3.2 Finite element model

The SHE has been simulated using a multi-linear thermomechanical model. This model adapts the stress-strain diagram when a temperature variation is applied, using the slope dσ/dT of the σ-T diagram (shown schematically in figure 25). Then, if the wire is subjected to a temperature variation ΔT, the model tracks the evolution of the transformation stress σ_{Ms} as follows:

$$\sigma_{Ms}^{T(i+1)} = \sigma_{Ms}^{T(i)} + (\Delta T \cdot \frac{d\sigma}{dT}) \qquad (2\text{-}10)$$

where the superscripts T(i+1) and T(i) denote the next and the current temperature respectively. If the wire is loaded from point (1) to point (2), the heat produced by the phase transformation shifts the transformation plateau toward higher stresses.

Due to its significant energy contribution (15 000 J/kg, see table II), the latent heat is expected to cause an important temperature variation (recoverable) and consequently an increase of the slope of the transformation lines (section 2.2.3). On the other hand, the energy contribution of internal friction is relatively small (around 1500 J/kg, see table II) and causes less temperature variation. However, because this energy is irrecoverable, the internal friction is responsible for the heat accumulation during repeated cycles (section 2.2.4).

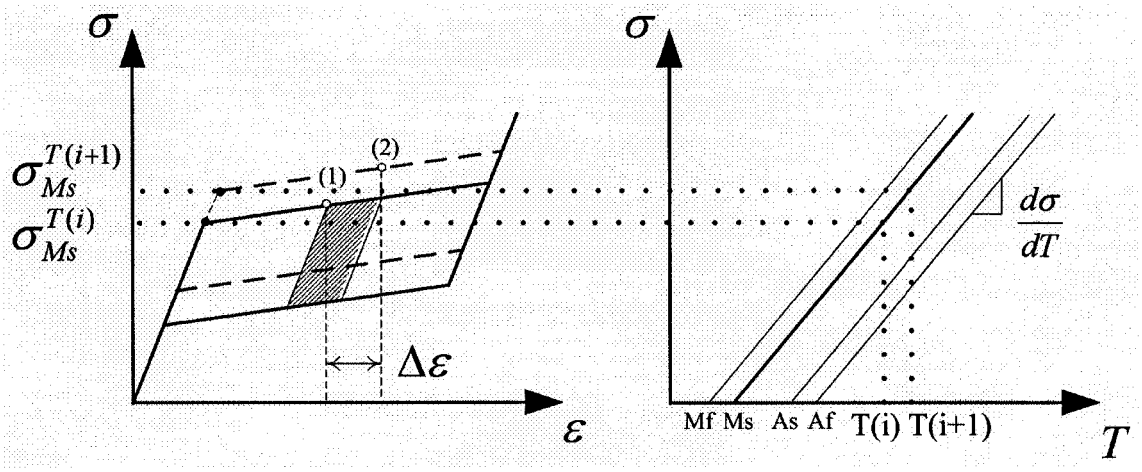

Figure 25 Effect of temperature on the thermomechanical model. The critical stresses (left) are adjusted with the stress-temperature relation defined by the state diagram (right).

The simulations are carried out using the general-purpose finite element software ANSYS 8.0. The material law described above is implemented using a user-defined subroutine. The wires are represented by a single tension-only spar element (LINK 180). The displacement of one end of the wire is controlled, while the other end is fixed. Table II gives the numerical values of the parameters used in the study.

Table II

Values of the coefficients used to simulate the SHE. (A): 0.1 mm wire; (B): 0.5 mm wire; (C): 2.46 mm wire

Symbol	Name	Value
ℓ	Transformation enthalpy	15 000 J/kg
ρ	Density	6500 kg/m^3
H	Area of hysteresis loop	1677 J/kg (A) 938 J/kg (B) 785 J/kg (C)
c	Specific heat	750 J/kg K
l	Length	60 mm (A, B) 134 mm (C)
$d\sigma/dT$	Clausius-Clapeyron coefficient	6.5 MPa/K (A, B) 5.93 MPa/K (C)

2.2.3.3 Results and discussion

The stress-strain curves and the temperature variation as a function of strain for the two types of small diameter wires are shown in figures 26 and 27 respectively. In figure 26, the experimental results are superposed on the numerical ones with a fairly good agreement. In figure 27, only calculated results were obtained due to the complexity related to the temperature measurement in thin wires. The arrows in figure 27 indicate if the wire is being loaded or unloaded.

The following observations can be made for the 0.5 mm wire (curves A, B, C in figure 26). For the 0.001 Hz loading, the equilibrium is practically established between the heat

produced by the transformation and the heat dissipated through the surface, leading to small temperature variations. This case is then considered as the quasi-static situation from which the transformation stresses and strains are used as inputs for the finite element model. For the 0.005 Hz case, more significant variations are observed during the loading. However, convection and radiation have enough time, when the transformation is over, to dissipate the heat, so that the wire reaches room temperature prior to unloading. During unloading, the wire absorbs some heat, and its temperature at the end of the cycle is below room temperature. As a result, the direct transformation stress plateau goes up and the reverse transformation stress plateau goes down (curve B compared to curve A in figure 26), increasing the width of the hysteresis loop. For the 1 Hz case, the temperature rise is very high (23 °C), so that the wire temperature always remains above room temperature. As a result, the slope of the phase transformation plateau increases and the width of the hysteresis loop decreases (curve C).

Similar observations can be made for the 0.1 mm wire (curves D, E, F in figure 26). However, for these wires, the direct transformation stress plateau shows a different behavior. Indeed, σ_{Ms} increases with the strain-rate, and a series of irregularities are experimentally observed in opposition to the smooth curves for the 0.5 mm wire.

As already suggested by Leo et al. [47], the presence of a single nucleation site leads to an energy barrier which has to be overcome at the onset of the phase transformation (rise in the transformation stress σ_{Ms}). Furthermore, Shaw [74] experimentally observed differences in the stress-strain behavior when nucleation appears at multiple sites instead of a single site. Torra et al. [75] also observed that distributed nucleation sites produce a smoother hysteresis without observing the occurrence of the phase transformation at a constant stress. Our hypothesis is then that the 0.5 mm wire has a distributed nucleation. This distribution is due to the heat treatment that was performed prior to testing. Therefore, the material is homogenized and many nucleation sites are available. That leads to a uniform temperature distribution and to a temperature rise proportional to the

fraction of the transformed martensite. This bulk (or distributed) heating does not cause the same rise of σ_{Ms} observed with the 0.1 mm wire (curves E, F), but a progressive increase of the transformation slope (curves B, C).

On the other hand, the 0.1 mm wire has a finite number of nucleation sites, probably created near the grips of the testing machine. A threshold force is then observed at the beginning of the transformation. This phenomenon is similar to the formation and the displacement of Lüders band in steel, i.e a significant force is necessary to initiate the nucleation [50;76]. In our case, the force is strain-rate dependent due to the Clausius-Clapeyron coefficient and, consequently, to the SHE.

These phenomena are very complex and depend on temperature, strain rate, strain amplitude, thermomechanical history, geometry of the sample and heat exchange conditions. However, even if these complex phenomena are neglected during modeling, it is shown in the following sections that it is possible to simulate the dynamic response of a structure equipped with SMA dampers. The objective is to obtain an acceptable coherence with experimental results for a given engineering application.

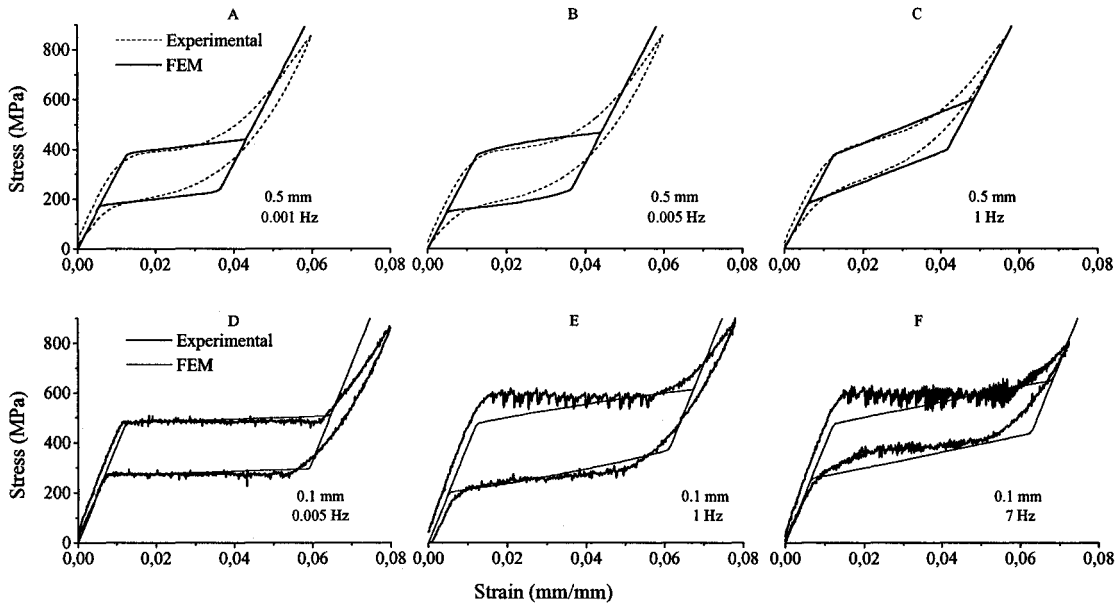

Figure 26 Stress-strain response for the 0.5 mm diameter (A-B-C) and the 0.1 mm diameter (D-E-F) for different stain rates. Numerical and experimental curves are superimposed.

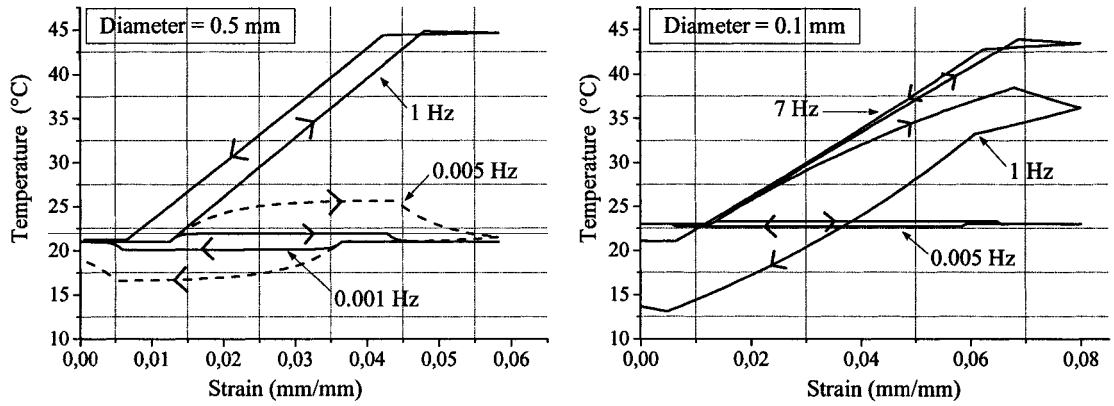

Figure 27 Numerically calculated temperature as a function of strain for the 0.5 mm diameter (top) and the 0.1 mm diameter (bottom) wires for the different strain rates.

2.2.3.4 Repeated cycles (large diameter NiTi wire)

The tests performed on the small diameter wires mainly underlined the contribution of the latent heat. This section will study the heat accumulation and the evolution of the pseudo steady state caused by the internal friction during repeated cycles.

The 2.46 mm diameter NiTi wire is experimentally cycled at 0.25 Hz for 200 seconds. The same experiment is numerically reproduced with the FEM. The wire is strained up to 5.5 % with a hydraulic tensile testing machine (MTS). The effective length of the wire is 134 mm. The temperature at the surface of the NiTi wire is measured by a thermocouple welded on the sample with copper-tin wire (Figure 28).

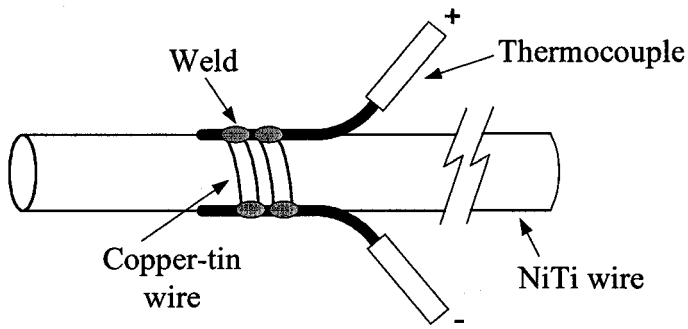

Figure 28 Thermocouple welded on the 2.46 mm diameter NiTi wire for the cycling test

The coefficient of heat exchange used in equation (2-5) has to be adjusted to take into account the fact that the free convection hypothesis is not suitable as a result of the movement of the ambient air (forced convection instead of natural convection). An exchange coefficient of 40 $W/(m^2 \cdot K)$ gives a good agreement with the experimental results. This h value has led to an insignificant temperature variation in the small diameter wire results. Figure 29 shows temperature variation with time. The temperature

oscillation is caused by the latent heat, while the increase of the average temperature is caused by the internal friction. The numerical and experimental results give a similar amplitude of the temperature oscillations (20 °C approx.), the same time constant (approx. 150 seconds) and the same stabilized temperature (32 °C).

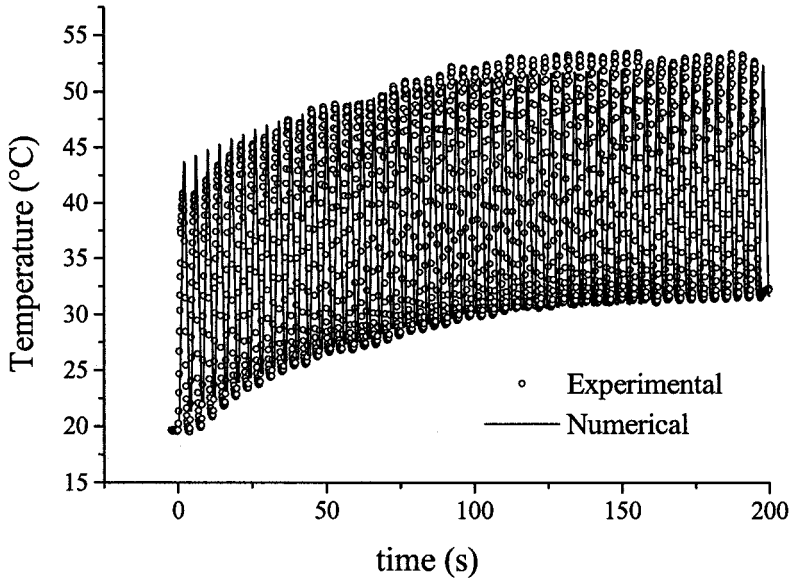

Figure 29 Experimental and numerical temperature variations with respect to time for a 2.46 mm diameter NiTi wire

2.2.3.5 Self-heating effect of a simple structure

The consequence of considering or not considering the SHE in a single degree of freedom (SDOF) structure is numerically analyzed here. The SDOF structure (figure 30) is a cantilever beam subjected to a harmonic oscillation. Two 0.5 mm NiTi wires restrain the beam. A mass is added at the free end, in such a way that the phase transformation is substantially initiated in the wires. Three different ways to account for the SHE (table III) are compared in figures 31 and 32. The first case includes the SHE via the heat balance formulation, as previously described, and the material constants of the multi-

linear model are taken from the quasi-static experiment (figure 26 A). The second case excludes the SHE and uses material constants also supplied by the quasi-static experiment (figure 26 A), completely excluding the dynamic effects. The last case also excludes the SHE, but instead uses the material constants supplied by the dynamic experiment (figure 26 C).

Table III

Summary of the different modeling cases

Modeling case	SHE	Type of experiment from which the material constants are obtained
1	Include	Quasi-static
2	Exclude	Quasi-static
3	Exclude	Dynamic

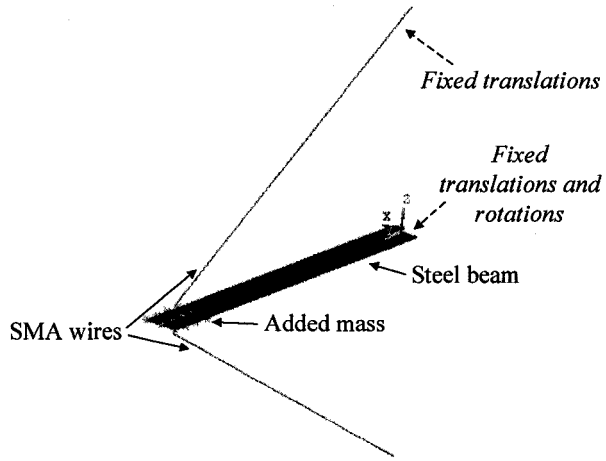

Figure 30 The finite element model of the SDOF structure used to study the SHE

The numerically calculated displacements of the free end are shown in figure 31 for the three cases (from 0.5 to 1 second). The first observation is that there is a difference between considering or not considering the SHE. However, it is clear that two cases are

very similar: considering the SHE via the heat balance with the quasi-static properties (case 1) or excluding it and using the dynamic properties (case 3).

The first three seconds of the displacement of the free end is plotted in figure 32 for the same three cases. It is observed that a difference between case 1 and case 3 now appears if the pseudo steady-state regime is simulated for a longer time. This is due to heat accumulation caused by the internal friction during the SHE calculations (case 1). However, the use of only the dynamic properties (case 3) is still a fairly good approximation.

These results suggest that different approaches can be applied for the preliminary design of a SMA damper. One of these approaches is to characterize the material by performing a dynamic loading (at room temperature) on the wire instead of using the heat balance calculations, which results in simpler and faster simulations. Another approach could be to characterize the material from a quasi-static loading (very low frequency) at a temperature above room temperature. Indeed, for larger diameter wires (for instance 2.46 mm), the characterization could be carried out at a temperature that is 30 K above room temperature in order to match the observations obtained with such wires reacting to a quake (for example during one minute with large deformations at frequencies close to -or over- 1 Hz).

In both approaches, if the sample's behavior remains inside its pseudoelastic window, the preliminary design is satisfactory even if the SHE calculations are neglected. However, the SHE calculations could be useful if there is significant heat accumulation, if the results of a dynamic characterization are not available, if more complex heat exchange conditions are present, or simply to evaluate the temperature rise of the wire during the loading.

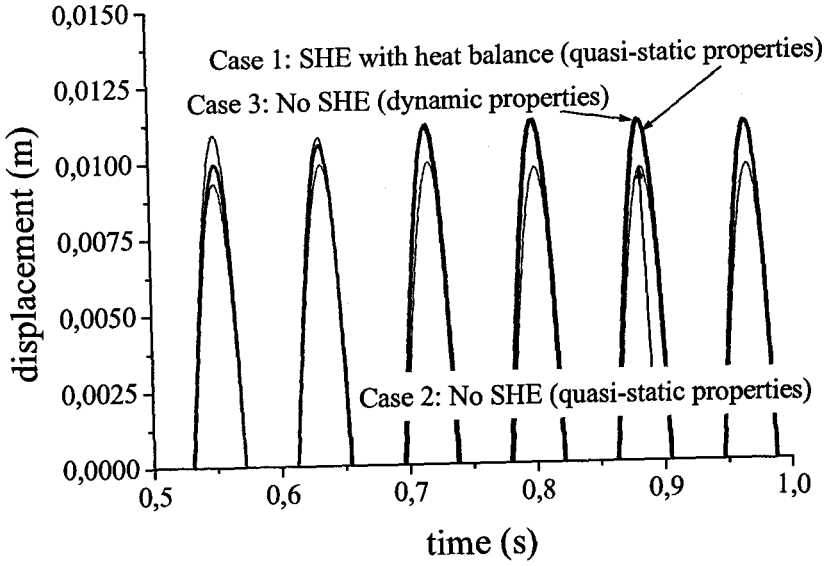

Figure 31 Displacement time history of the SDOF structure subjected to a harmonic oscillation (during the first second)

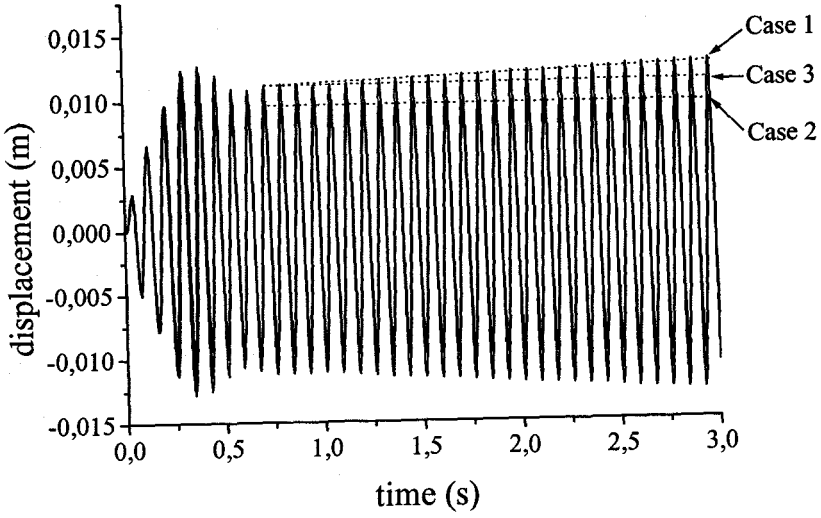

Figure 32 First three seconds of displacement time history of the SDOF structure subjected to a harmonic oscillation

2.3 Superelastic origins of damping

It is well known that the superelasticity of SMA can be judiciously exploited in the design of dampers. Unfortunately, it is not clear if these benefits come from the stiffness variation and/or the energy dissipation that are inherent to a superelastic cycle. This section studies a SDOF structure subjected to a harmonic solicitation in order to get a better understanding of this matter. A FEM of the structure will first be validated. Then, a numerical study will be used to analyze the effect of the superelastic properties on the response of the structure.

2.3.1 Test protocol

2.3.1.1 Experimental

The structure used here (figure 33) is a horizontal beam (thin steel plate, length of 400 mm) with two 70-grams masses added at its ends. The rigid columns are made of round aluminum bars (length of 120 mm). Four SMA wires with diameters of 0.1 mm are used to damp the system. The assembly is mounted on a testing machine that controls the displacements of the upper part of the structure. The structure is symmetric with respect to its vertical axis in order to equilibrate the forces and to minimize the horizontal displacement of the lower part of the setup. The displacement generated by the testing machine is measured with its internal LVDT, while the displacement of the beam's free end is measured with a laser sensor (model CP35 manufactured by Wangler). The relative displacement of the mass is obtained by the subtraction of these two displacements.

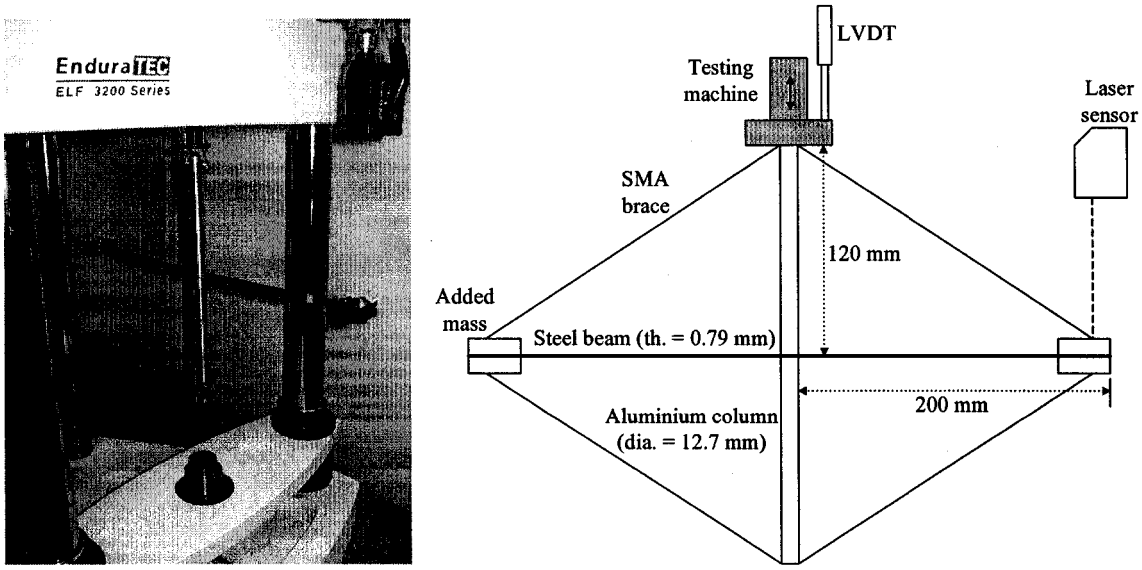

Figure 33 Experimental test setup and structure

The testing machine produces a sine wave as the input motion signal. Four series of tests at different peak accelerations are performed on the structure (a = 0.75, 1, 1.25 and 1.5 g). For each series, the frequency of the sine wave (f) is swept from 8 to 15 Hz (range of the testing machine) with an increment of 1 Hz or 0.5 Hz near the natural frequencies. To keep the peak acceleration constant for a series of tests, the peak displacement (x) of the head is obtained by:

$$x = \frac{a}{4 \cdot \pi^2 \cdot f^2} \tag{2-11}$$

Note that for each experiment, new precycled wires are installed. A first dynamic test is also performed to ensure that there is no residual drift and that the setup is stable.

2.3.1.2 Numerical

The same experiments are realized with ANSYS, a finite element analysis software. Only one half of the structure is represented and the columns can be omitted if proper boundary conditions are set (figure 30). Shell elements are used to represent the beam. Mass elements simulate the added mass, while the SMA braces use a link element with user programmable features (LINK 180). The damping ratio of the structure is determined by performing a free decrement test. Rayleigh damping coefficients are adjusted on the model to fit the experimental test ($\alpha = 0.0095$, $\beta = 0.0016$). Finally, the dynamic test of figure 26 F is used to characterize the behavior of the wires, and the heat balance calculations are omitted.

2.3.2 Validation of the model

The dynamic amplification of the structure (D) is defined as the ratio of the dynamic displacement amplitude to the static deflection [4]. For a given value of input acceleration, the values of D are plotted with respect to the input frequency. Figure 34 gives an example for the 1.25 g test. The natural frequency of the system (f_n) and the value of D at that frequency (D_n) are reported in figures 35 and 36 respectively for all the input accelerations tested.

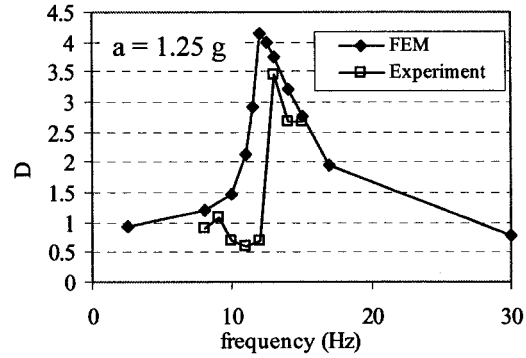

Figure 34 Numerical and experimental frequency response of the structure for input acceleration of 1.25 g

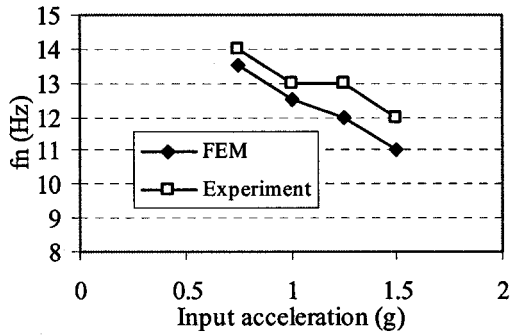

Figure 35 Numerical and experimental natural frequencies for all the input accelerations tested

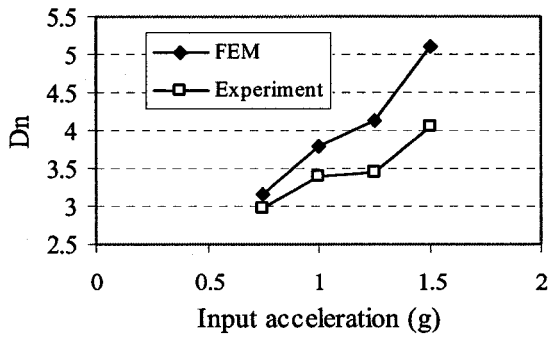

Figure 36 Numerical and experimental dynamic amplification at the natural frequencies for all the input accelerations tested

Figure 35 shows that the values of f_n decrease for higher input accelerations, which denotes a reduction of the global stiffness of the structure due to the phase transformation. The overestimation of D_n and the underestimation of f_n by the FEM are probably caused by modeling of boundary conditions. Actually, the free end of the experimental setup showed a slight lateral displacement while the FEM considered it as fixed. In spite of these differences, the FEM results seem to be reliable enough for the numerical analyses to be carried further.

2.3.3 Energy dissipation vs variable stiffness

Two relevant characteristics of superelastic SMA can be responsible for their good damping properties: the energy dissipated by the hysteresis loop and the variation of the stiffness caused by the phase transformation. Here, the FEM model described in figure 25 is used to analyze the effect of those parameters. To this end, three different 'materials' are used. The first one is the SE material previously used in figure 37 A. The second one is a hypothetic linear material that has the same initial stiffness as the SE material (no phase transformation) (figure 37 B). The third one is also a hypothetic multi-linear elastic material that has the same loading behavior as the SE material. However, no hysteresis is considered so that a "zero energy dissipation" (ZED) material is obtained (figure 37 C).

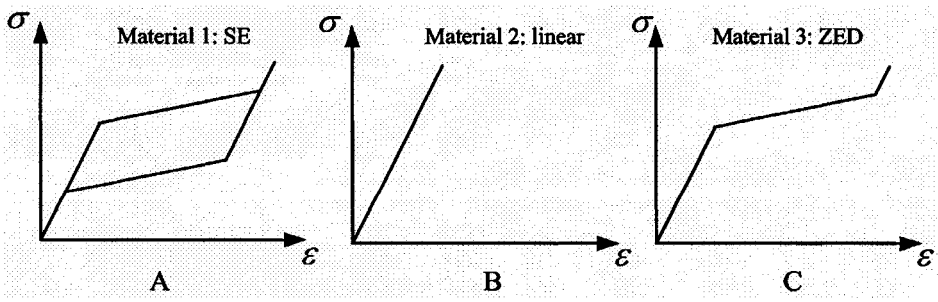

Figure 37 The different material models tested

The values of D_n are shown in figure 38 for different input accelerations and for the three material models. For a low acceleration value (0.5 g), the phase transformation is not initiated and the three models give the same Dn. For accelerations of 1, 1.25, 1.5 and 1.75 g, the best material is the linear one. This result suggests that the energy dissipated by the SE material cannot compensate for the reduction in the stiffness encountered during the martensitic transformation. Also, the SE material shows better results than the ZED material. There are two reasons for this: (a) the energy dissipated by the hysteretic loop and (b) the higher stiffness of the SE material during the internal subloops as compared to the constant stiffness of the ZED in its transformation regime. The relative contribution of each of these phenomena remains to be quantified.

From these results, it can be concluded that to minimize the displacements, a compromise between the stiffness and the energy dissipation should be found by adjusting the thermomechanical processing and possibly the alloy's composition. For example, a material with a high transformation stress instead of a large hysteretic loop could be used for certain applications. NiTi alloys that developed stresses up to 1500 MPa with a small hysteresis width have been developed [41;77]. Such stresses are of the same order of magnitude as the maximal stress supported by the linear dampers during the 1.75 g test (1400 and 1600 MPa). In civil engineering, this situation corresponds exclusively to a re-centering system instead of a damper. Furthermore, if used as a tendon in a connection, the transformation plateau present in these materials can be used to limit the stress on the member's structure.

The previous analysis is based on the reduction of the maximal displacement. If the maximum acceleration is analyzed instead (the acceleration is obtained by double derivation of the displacement), the SMA gives smaller accelerations than linear elastic or ZED material (figure 38). Therefore, the material characteristics have to be judiciously chosen in order to obtain the desired response from the damping/re-centering system for a particular application.

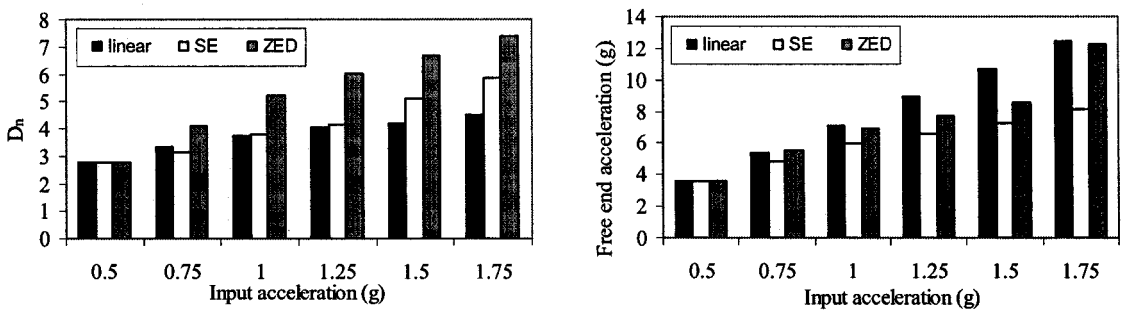

Figure 38 Comparison of the material models' dynamic amplification (left) and free end accelerations (right) for different input accelerations

2.4 Conclusion

The first part of this study investigates the self-heating effect of SMA. This phenomenon has been implemented in a commercial finite element software and the model has been validated by testing three different wires. It has been shown that the use of the material parameters determined by dynamic tests could be equivalent, in some situations, to more complex calculations involving the self-heating effect.

The second part of this work studies the respective effect of the stiffness variation and the energy dissipated by a superelastic material. To this end, a FEM of a single degree of freedom structure was used. The FEM have been validated by experimental tests. The numerical results showed that the displacements of the structure are smaller when a purely linear material is used instead of the SE material, since the overall stiffness of the linear model is larger than that of the SE model. However, the SE material represents a better choice compared to a multi-linear material without a hysteresis for both the maximal displacement and acceleration. The SE material is also better than a purely elastic material in terms of the maximal acceleration. Therefore, superelastic shape memory alloy dampers constitute a good technical solution for structural dampers, while also acting as re-centering devices.